Optical Efficiency of Feedhorn-Coupled TES Polarimeters for Next-Generation CMB Instruments

J. W. Henning[a], J. W. Appel[b], J. E. Austermann[a], J.A. Beall[c], D. Becker[c], D. A. Bennett[c], L. E. Bleem[d], B. A. Benson[d], J. Britton[c], J. E. Carlstrom[d], C. L. Chang[d], H. M. Cho[c], A. T. Crites[d], T. Essinger-Hileman[b], W. Everett[d], E.M. George[e], N. W. Halverson[a], G. C. Hilton[c], W.L. Holzapfel[e], J. Hubmayr[c], K. D. Irwin[c], D. Li[c], J. McMahon[f], J. Mehl[d], S. S. Meyer[d], S. Moseley[g], J. P. Nibarger[c], M. D. Niemack[c], L. P. Parker[b], E. Shirokoff[e], S. M. Simon[a], S. T. Staggs[b], J. N. Ullom[c], K. U-Yen [g], C. Visnjic[b], E. Wollack[g], K. W. Yoon[c], E.Y. Young[e], Y. Zhao[b]

[a]Center for Astrophysics and Space Astronomy, Department of Astrophysical and Planetary Sciences, University of Colorado, Boulder, CO 80309, USA;

[b] Department of Physics, Princeton University, Joseph Henry Laboratories of Physics, Jadwin Hall, Princeton, NJ, 08544, USA;

[c]NIST Quantum Devices Group, 325 Broadway Mailcode 817.03, Boulder,CO 80305, USA;

[d]Kavli Institute for Cosmological Physics, University of Chicago, 5640 S. Ellis Ave., Chicago, IL 60637, USA;

[e]Department of Physics, University of California, 366 LeConte Hall MC 7300, Berkeley, CA 94720, USA;

[f]Department of Physics, University of Michigan, 450 Church St., Ann Arbor, MI 48109, USA;

[g]NASA Goddard Space Flight Center, Mail Code 665, Greenbelt, MD 20771, USA

ABSTRACT

The next generation of Cosmic Microwave Background (CMB) experiments probing for signals of inflation and small angular scale polarization anisotropies require higher sensitivity and better control of systematics. We are developing monolithic arrays of orthomode transducer (OMT) coupled transition edge sensor (TES) polarimeters designed for operation at 150 GHz to address these requirements. OMT coupling allows for simultaneous and independent detection of two orthogonal linear polarization states incident on a single pixel. We present measurements of optical efficiencies $\eta_{\rm op}$ of single pixels with on-chip band-defining filters, with $\eta_{\rm op} = 57 \pm 4\,{\rm stat} \pm 9\,{\rm sys}$ %. We also provide evidence for an out-of-band blue leak and address possible sources as well as mitigation techniques. Additionally, we discuss methods for increasing efficiency being implemented in the next generation of pixels, currently in fabrication. Still under development, these pixels are produced as monolithic polarimeter arrays and are slated for use in the Atacama Cosmology Telescope Polarization (ACTpol) and South Pole Telescope Polarization (SPTpol) experiments, while single-pixel polarimeters are to be deployed in the Atacama B-mode Search (ABS) experiment.

Keywords: TES, bolometer, polarimeter, detector array, optical properties, cosmology

1. INTRODUCTION

In addition to temperature anisotropies, measurements of polarization in the CMB hold promise for revealing new information about the initial conditions of the universe. E-mode polarization has been observed[1–5] and recent experiments are beginning to find statistically significant structure in the EE auto-correlation and TE cross-correlation power spectra. B-mode polarization, however, has yet to be detected.[6] Because the only known theoretical source of B-mode polarization at large angular scales is gravitational waves from the epoch of

Millimeter, Submillimeter, and Far-Infrared Detectors and Instrumentation for Astronomy V,
edited by Wayne S. Holland, Jonas Zmuidzinas, Proc. of SPIE Vol. 7741, 774122
 · doi: 10.1117/12.859478

inflation,[7] the B-mode signal, if detected, holds the potential of revealing information not only about structure formation and the distribution of matter in the universe, but also the energy scale of inflation. Additionally, B-modes are also expected to be sourced at smaller angular scales by gravitationally lensed E-mode polarization, which along with placing tighter constraints on ΛCDM and derived cosmological parameters will also provide strong limits on the total of neutrino masses.

The most optimistic theoretical models predict B-mode signals from inflationary gravitational waves to be at least an order of magnitude smaller than current 95% confidence upper limits,[6,8] which are themselves five and half orders of magnitude smaller than the peak amplitude in the spectrum of primary CMB *temperature* anisotropies. A successful detection of B-mode polarization will require kilopixel-sized arrays of nearly background-limited detectors that present a high degree of uniformity in their electrothermal and readout properties. Efficient use of telescope time will also be essential to detect the faint B-mode signal in a reasonable timeframe. Therefore, a high optical efficiency is an attractive property for next-generation polarimeters.

Researchers at the University of Colorado at Boulder, Princeton University, NIST-Boulder, the University of Chicago, the University of California at Berkeley, the University of Michigan, and NASA Goddard Space Flight Center have been developing mm-wave polarimeter arrays utilizing transition edge sensor (TES) bolometers for CMB polarization experiments as the TRUCE Collaboration. These detector arrays will be used in the ABS,[9] SPTpol,[10] and ACTpol[11] experiments. In this article, we report on measured optical efficiencies of the most recently tested prototype pixel generation. We also present evidence for and address continuing efforts to mitigate an out-of-band "blue" power leak.

The most recently tested prototype pixel is briefly described in Section 2. We describe the blackbody source and testing techniques used to calculate optical efficiencies in Section 3, followed by efficiency results and evidence for a blue leak in Section 4. Section 5 explores possible sources for the blue leak and discusses both ways to mitigate the leak and increase the optical efficiency in the next generation of devices. We conclude in Section 6.

2. THE PIXELS

The most recent prototype pixel design (CMB5) is shown in Figure 1. Incident light is feedhorn-coupled to a 1.6 mm orthomode transducer (OMT) that splits the signal into two orthogonal polarization states. The light is then propagated through coplanar waveguide (CPW) and finally lossless Nb microstrip to two TESs (hereafter A and B). Each TES is thus sensitive to a single polarization state. A third "dark" TES (TES D) is also included for characterizing electrothermal properties, calibrations, and controlling systematics. To define the passband, quarter-wave stub filters are included in the lithographed lines. Currently, the passband is centered at 145 GHz with a fractional bandwidth of $\sim 25\%$. Having band-defining filters on-chip is a key feature of these pixels. With this technology, the requirement for specific band-defining filter stacks upstream in the instrument optics is relaxed, allowing for the powerful option of multichroic monolithic arrays. Observations of multiple bands are necessary to remove astrophysical foreground contaminants, and simultaneous multi-band observing can reduce total integration time by a factor up to the number of simultaneous bands.

Each TES is thermally isolated by floating on a relieved silicon nitride island supported by nitride legs, the dimensions of which determine the thermal conductance G of the device. An Au meander surrounding the TES itself provides area for the signal to be converted to heat, which is sensed by the TES. A small Au heater is also included on the TES island for further characterization and calibration of the detector. As currently designed the TESs have critical temperatures $T_c \sim 540$ mK, normal resistances $R_n \sim 5\,\mathrm{m}\Omega$, and thermal time constants $\tau \sim 2.6$ ms.[12] The CMB5 generation was fabricated in two groups, one with low G ($\sim 65-70$ pW/K) and one with high G ($\sim 500-600$ pW/K) and is measured to have dark NEP consistent with phonon noise at $\sim 3\times10^{-17}\,\mathrm{W}/\sqrt{\mathrm{Hz}}$ for low-G pixels and $\sim 7\times10^{-17}\,\mathrm{W}/\sqrt{\mathrm{Hz}}$ for high-G pixels.[12]

3. APPARATUS AND METHODS

3.1 Temperature-Controlled Cold Load

We have designed and built a temperature-controlled blackbody cold load for simultaneous optical efficiency measurements of several detectors. We define optical efficiency as the ratio of power measured by the detectors

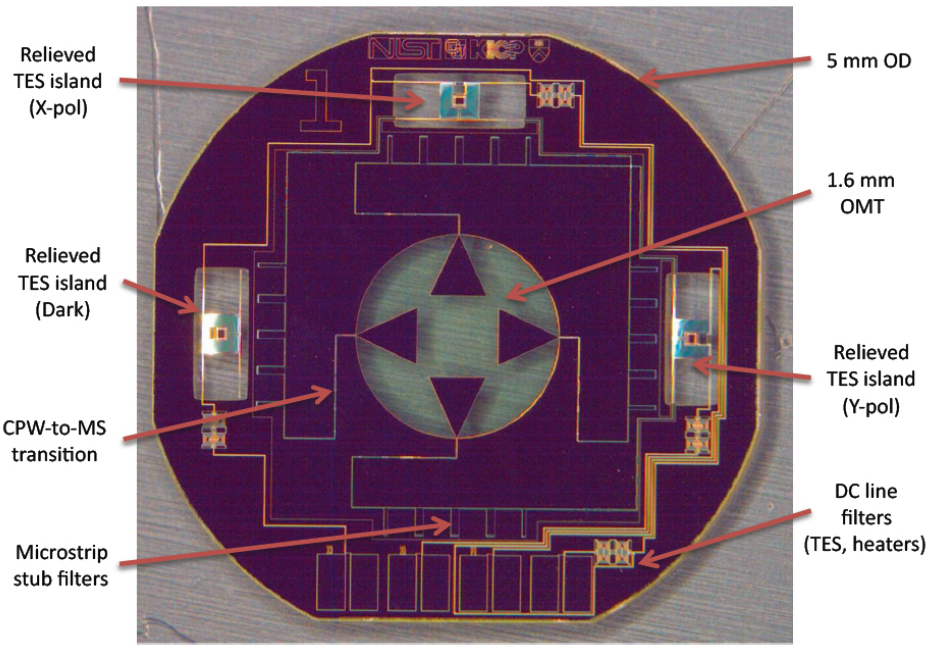

Figure 1. A low-G CMB5 pixel. 5 mm across, the pixel consists of a ⌀ 1.6 mm OMT that couples orthogonal polarization modes to two separate optically coupled TES bolometers. (TES A, or X-pol, and TES B, or Y-pol). A third dark (D) TES is included for studies of electrothermal properties, characterization, and control of systematics. Quarter-wave stub filters built into lossless Nb microstrip lines define the bandpass of observation to be 120 - 175 GHz. Figure also appears in Yoon, et al. 2009.[13]

to that of the total in-band incident power coupling to the feedhorns. Unlike an external load, the "cold" load is positioned next to detectors in the 4 K volume of a testing cryostat and can be heated to more than 60 K, functionally limited in temperature due to decreased mK stage hold times. The load is positioned approximately 7 mm from individual pixel feedhorns, which allows for the simplest possible optical path and reduces complication of the analysis and interpretation of measurements. The horns fit inside an Al 1100 alloy radiation shield sunk to 4 K surrounding the blackbody load. The radiation shield is coated with Bock black[14] on the inside to absorb non-coupled radiation and covered in aluminum tape on the outside to reduce emissivity.

The emitting material of the load is eccosorb CR-110.[15] Eccosorb is an iron-loaded plastic base epoxy with a relatively low power reflectance[16] and a large heat capacity.[17] G-10 standoffs are used to thermally isolate the eccosorb from the 4 K plate. The eccosorb heat capacity C and thermal conductance G of the standoff legs give the load an effective time constant τ of roughly 10 minutes, which precludes rapid temperature modulation during testing. Thermal fluctuations and systematics on these timescales limit accuracy at low temperatures (less than ~ 15 K) but improve with temperature as the fractional thermal drift becomes small.

The load is heated by four resistors encased in stycast. These are thermally sunk to the back side of a copper plate on which the eccosorb is mounted to improve load isothermality. Two DT470 Lakeshore diode thermometers are varnished to opposite corners of the eccosorb to measure the load temperature. Finally, a third diode is externally attached to the radiation shield to monitor its temperature. A picture of the load before complete installation of the horns is provided in Figure 2.

3.2 Optical Efficiency Measurements

The change in power a TES absorbs is measured by monitoring the bias power $P_{\rm TES}$ needed to keep the device in its superconducting transition as the temperature of the cold load $T_{\rm L}$ is varied; as incident optical power increases with load temperature the required electrical bias power decreases. To measure $P_{\rm TES}$ of a device at a single load temperature we servo control the pixel bath to 300 mK, well below the $T_{\rm c}$s of the TESs. The current

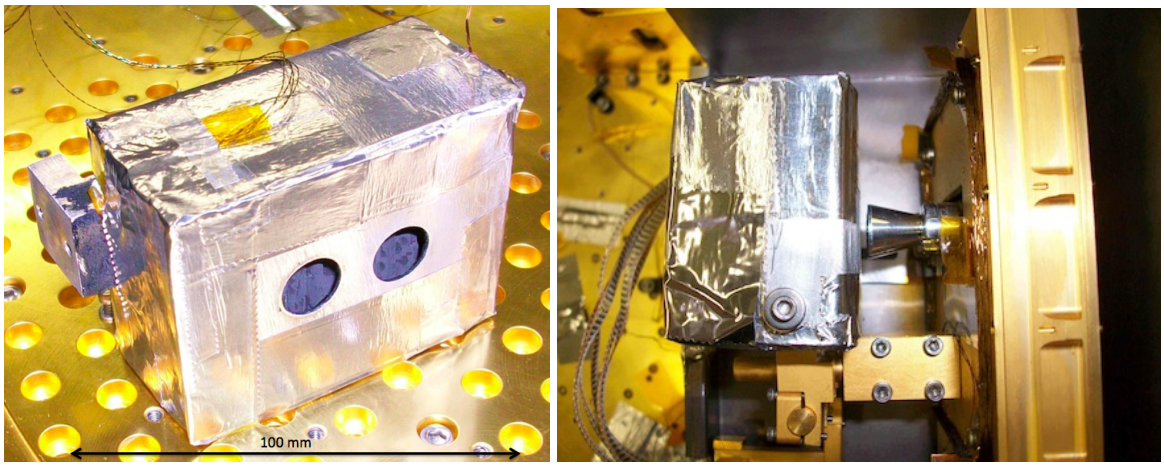

Figure 2. (Left) The cold load before installation resting on the 4 K plate. The eccosorb is visible through feedhorn holes in the Al 1100 radiation shield. (Right) The load installed in front of horns, which are later partially inserted within the load shield. Each horn is attached to an individual pixel mounted inside a gold-plated copper box thermally sunk to the mK stage.

through a device is monitored during a sweep of applied electrical bias voltages (an IV curve), taking the device from normal behavior through most of its superconducting transition. Calibrating the curve gives TES resistance ($R_{\rm TES}$, with $R_{\rm n}$ being the normal resistance of the device), the current applied to the device ($I_{\rm TES}$), and the voltage across the device ($V_{\rm TES}$) throughout the transition. $R_{\rm TES}$ is then plotted as a function of the bias power supplied $P_{\rm TES} = V_{\rm TES} I_{\rm TES}$. The difference in $P_{\rm TES}$ between different load temperatures should be constant at every point in the superconducting transition. Therefore, the average of $\Delta P_{\rm TES}$ between 55 and 80% $R_{\rm n}$ is taken, where the transition is approximately linear. The lower limit 55% is an artifact of our observations; we do not routinely monitor deeper into the transitions.

The power radiated by a nearly blackbody load that couples via a single-moded waveguide to a TES sensitive to one polarization mode is straightforward to calculate:

$$P_{\rm L} = \int \epsilon A_{\rm T} f(\nu) \frac{2h\nu^3}{c^2} \frac{1}{e^{\frac{h\nu}{kT_{\rm L}}} - 1} d\Omega d\nu. \tag{1}$$

Here, ϵ is the effective load emissivity, $A_{\rm T}$ is the throughput as a function of angular position, and $f(\nu)$ is the filter response function defined by the stub filters on the pixels. For single-moded feedhorns, the throughput integrates to just $\lambda^2/2$, which reduces Equation 1 to

$$P_{\rm L} = \int_{\nu_0}^{\nu_1} \epsilon f(\nu) \frac{h\nu}{e^{\frac{h\nu}{kT_{\rm L}}} - 1} d\nu, \tag{2}$$

where ν_0 and ν_1 are the edges of the bandpass.

Comparing $P_{\rm TES}$ to the change in outputted in-band load power $P_{\rm L}$ at two different load temperatures T_1 and T_2 provides the optical efficiency, via

$$\eta_{\rm op} = \frac{\Delta P_{\rm TES}}{\Delta P_{\rm L}} = \frac{P_{\rm TES}(T_1) - P_{\rm TES}(T_2)}{P_{\rm L}(T_2) - P_{\rm L}(T_1)}. \tag{3}$$

The sign of $P_{\rm TES}$ is reversed since electrical bias power drops with increasing incident optical power. The total incident power on detectors required to bias the devices to a single point in their transitions is constant (a byproduct of operating the devices in voltage-biased mode which takes advantage of strong negative electrothermal feedback). By measuring $P_{\rm TES}$ at many cold load temperatures one obtains several measurements of $\eta_{\rm op}$, which must satisfy

$$\mathrm{C} = P_{\rm TES}(T_{\rm L}) + \eta_{\rm op} P_{\rm L}(T_{\rm L}). \tag{4}$$

4. RESULTS

The left of Figure 3 plots the negative change in bias power measured for each TES with respect to measurements at $T_{\rm L} = 4$ K at every load temperature, with 5% systematic errors from uncertainties in readout resistance calibrations. Additionally, the total in-band cold load power incident on TES A and B is plotted with error bars resulting from a systematic uncertainty of 250 mK in load temperature. It is clear from the plots for both high-G (top) and low-G (bottom) pixels that significant power is also coupling to the dark TES (D). This detector should be largely uncoupled to in-band radiation, so the observed signal is likely out-of-band power coupling by a different mechanism. Indeed, FTS measurements made by collaborators at the University of Chicago on different pixels from this fabrication generation reveal a considerable "blue leak" in the pixel filter response function[18] (Figure 4). Total out-of-band coupling is temperature-dependent but accounts for roughly 50% of the total absorbed power at 35 K, (see Section 5). The cause of the blue leak is still being investigated, but evidence suggests it is coupling directly to the TES islands through reflections in open-air cavities above and below pixels mounted for optical testing.

Recent tests at the University of Colorado and Princeton reveal that filling the cavity above and below the pixels with an absorbing eccosorb moat attenuates the high frequency leak by roughly half. The bottom left of Figure 4 shows two runs of efficiency measurements for the same dark TES on the high-G pixel, one with no moat and one with a moat above the pixel, clearly indicating a reduction in the out-of-band response by more than a factor of two. The bottom right figure shows the effects of the addition of a moat beneath the pixel as well as above. This helps to further mitigate the dark response at higher load temperatures. It should be noted that all three experiments slated to use these pixels (ABS, ACTpol, and SPTpol) have plans for optical low-pass filters in their optics, making any unresolved blue passband leak inconsequential to the operation and success of the experiments and the achievement of their science goals.

The blue leak complicates our assumption that throughput is simply $\lambda^2/2$ for each polarization mode. At

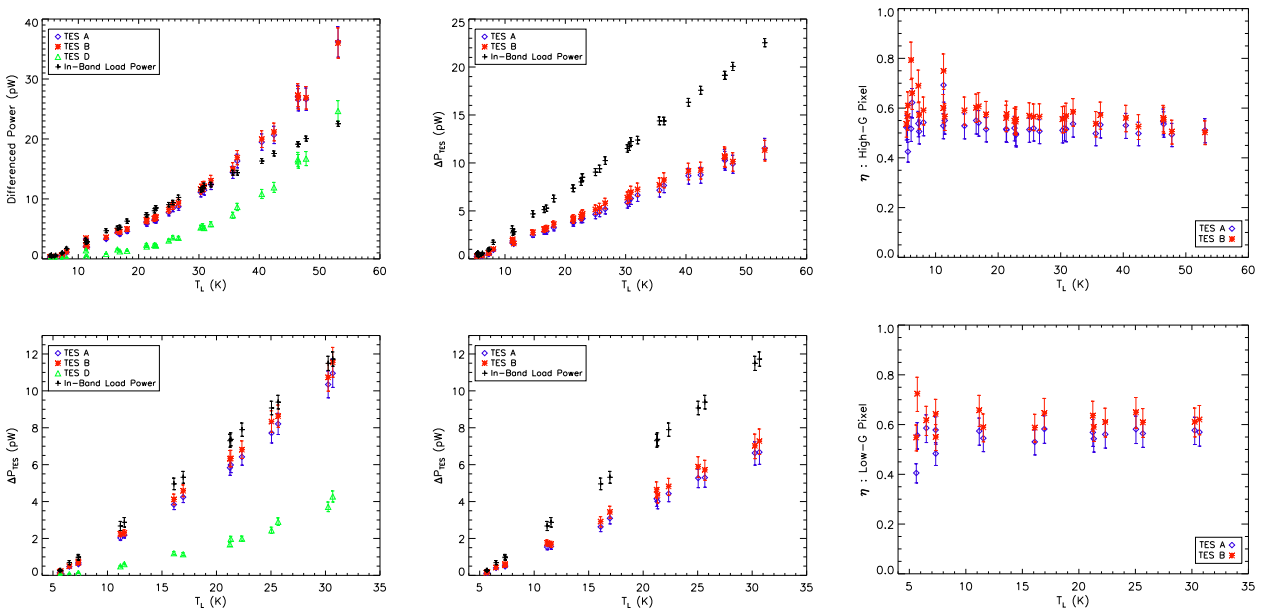

Figure 3. (Top Left) ΔP levels for the cold load and all three TESs in one high-G pixel. In-band load power is calculated as the incident power on the detector coupled through a lossless device, including the waveguide and bandpass filters. Note the significant coupled power to TES D, indicating an out-of-band leak. (Top Center) Same as the left, with $P_{\rm TES,\,D}$ subtracted from $P_{\rm TES,\,A\,or\,B}$ for the high-G device. (Top Right) Compilation of optical efficiency measurements for one high-G pixel. Variations in measured efficiency (due to long time constant thermal variations in the load) are smaller at higher temperatures due to reduced fractional changes in load power since $P_{\rm L} \sim T^4$. (Bottom) Same as above, but for one low-G pixel. Error bars are for systematic uncertainties resulting from common calibration errors.

frequencies beyond the desired bandpass, the horns and waveguide are no longer single-moded, further weighting throughput by ν or ν^2. In principle, however, the power coupling to TES D is entirely out-of-band. If the out-of-band power has an equal chance of being absorbed by all three bolometers on a pixel, then subtracting the dark TES power from the powers of TES A and B should leave only the in-band power detected by the devices. The middle and right plots of Figure 3 show $P_{\mathrm{TES,\,A\,or\,B}}$ after subtraction of $P_{\mathrm{TES,\,D}}$ and the resulting optical efficiency η_{op} values versus cold load temperature, respectively. If we assume subtracting TES D power completely removes the blue leak contribution to TES A and B, upon averaging the efficiencies the mean results with standard deviations for detectors A and B for both the high-G and low-G pixels are

$$\bar{\eta}_{\mathrm{A,\,high}} = 0.53 \pm 0.04 \quad ; \quad \bar{\eta}_{\mathrm{B,\,high}} = 0.58 \pm 0.06, \tag{5}$$

$$\bar{\eta}_{\mathrm{A,\,low}} = 0.55 \pm 0.05 \quad ; \quad \bar{\eta}_{\mathrm{B,\,low}} = 0.62 \pm 0.04, \tag{6}$$

where "high" and "low" denote high-G and low-G pixels, respectively. Averaging the four efficiencies gives $57 \pm 4\,\mathrm{stat} \pm 9\,\mathrm{sys}$ %. This agrees favorably with results from measurements at Princeton University, where 55% efficiency was calculated for a single TES optically coupled via copper and stainless steel waveguide to a cold load heated up to 25 K.[18]

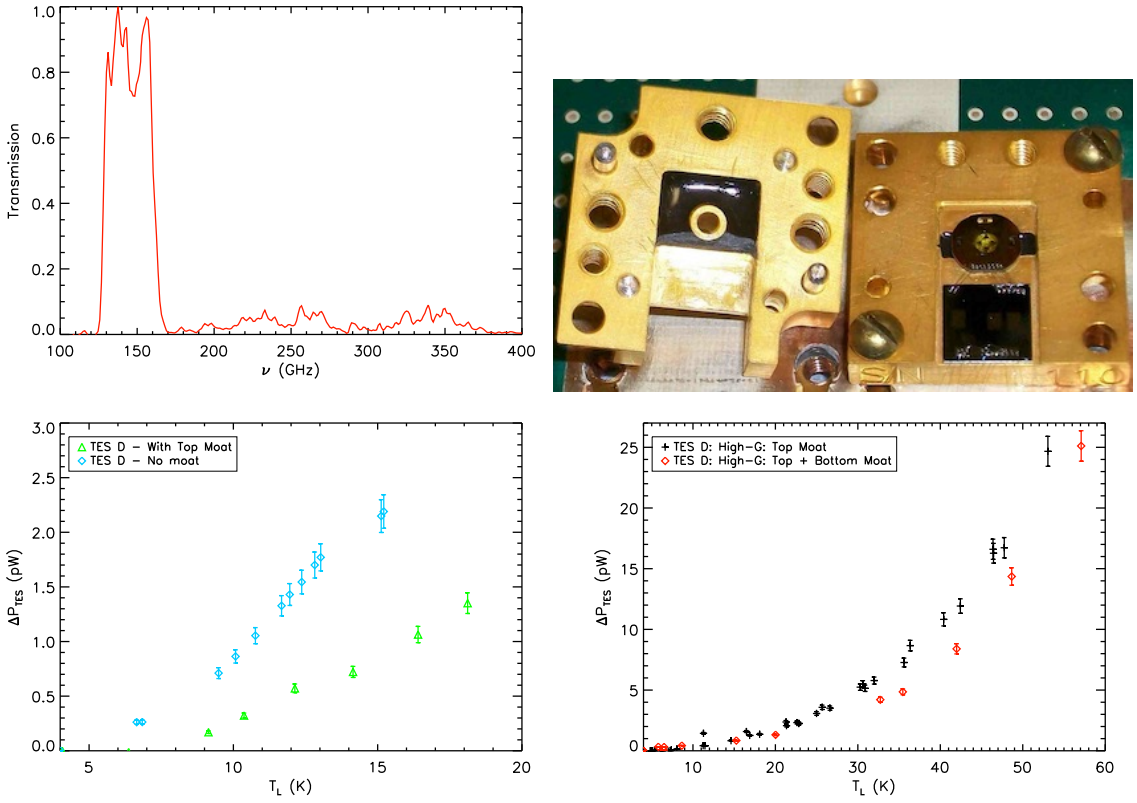

Figure 4. (Top Left) FTS measurements of stub filter transmission out to 400 GHz,[18] arbitrarily normalized to the peak transmission. In-band variation of transmission is an artifact of experimental setup and is not intrinsic to the band. The "blue" leak is largest out to 400 GHz, but continues to at least 2 THz, accounting for roughly 50% of the total absorbed TES power at 35 K. (Top Right) Eccosorb moats above and below the mounted pixels reduce the absorbed blue leak power by roughly half. (Bottom) Effect of top moat only compared to no moat on a high-G dark TES response (Left), and the effect of both a bottom and top moat compared to just a top moat (right). Error bars are systematics based on readout calibration uncertainties.

5. DISCUSSION

All pixels tested with this experimental setup exhibit a systematic difference in the optical efficiencies between TES A and B of a few percent, both in high- and low-G pixels. One possible explanation is that the load itself is slightly polarized, favoring one optically coupled TES over the other. Grooves in two directions on the surface of the eccosorb were sculpted by hand to reduce specular reflections and polarization but were not optimized to do so. A future larger version of the load, which will test large fractions of 84 pixel arrays, will instead use tessellating THz radar absorbing material (RAM) tiles developed by Thomas Keating Instruments that demonstrate reflected polarized power at less than -30 dB.[19]

Apart from a slight difference in efficiencies between TESs, the average absolute efficiency is perhaps lower than desired but not prohibitively so for the science goals in question, and several changes have been implemented in the next generation of pixels currently in fabrication (CMB6) to increase the efficiency even more. From HFSS simulations, we expect to gain roughly 5% efficiency from more careful impedance matching between the OMT and the CPW. Fabrication procedures have been modified to produce more vertical sidewalls in the Nb microstrip; non-vertical sidewalls allow the chance for edges of the microstrip to go normal and dissipate coupled power before it reaches the TES islands. Finally, the Au meander on the TES islands has been thickened to improve power dissipation.

Differences in absorbed out-of-band power between high- and low-G pixels corroborate results from using eccosorb moats in indicating the blue leak is possibly related to the area of the TES nitride islands. The blue leak is worse in high-G pixels, where the aspect ratio of the island legs needed to increase G also increases the total area of the island with respect to the low-G pixels. The known ratio of island areas between high- and low-G pixels is 1.64. If the blue leak is proportional to island area A then one would expect the ratio of out-of-band (TES D) to total (TES A or B) responses to be

$$\frac{P_{\mathrm{TES,\,D}}}{P_{\mathrm{TES,\,A\,or\,B}}} \propto A\,T_{\mathrm{L}}^{\alpha}. \tag{7}$$

The power law index α will change according to how much of the blue leak passband is in the Rayleigh-Jeans (RJ) limit. When the leak is fully in the RJ limit, both in-band and out-of-band power scale linearly with T_{L} so $\alpha = 0$. Blackbody power calculations factoring in the blue leak up to 2 THz, however, suggest the RJ limit isn't reached until $T_{\mathrm{L}} \sim 200$ K. Figure 5 shows D/A and D/B responses for both high- and low-G pixels. For simplicity, solid (dashed) lines are linear fits to D/A (D/B) for both pixel types at temperatures above 15 K (to avoid ΔP_{L} fluctuations larger than 10% due to small thermal variations in the load). If in fact the blue leak is dependent on island area and Equation 7 holds (with α assumed to be 1) then the slopes of the lines are proportional to the area of the nitride islands. The ratio of slopes for D/A and D/B are

$$\frac{A_{\mathrm{high,\,A}}}{A_{\mathrm{low,\,A}}} = 1.70 \pm 0.43\,\mathrm{stat} \qquad : \qquad \frac{A_{\mathrm{high,\,B}}}{A_{\mathrm{low,\,B}}} = 1.72 \pm 0.43\,\mathrm{stat}. \tag{8}$$

The large statistical errors likely can be improved by using more sophisticated modeling, but a linear fit is nevertheless illustrative. As anticipated, these ratios are consistent with the known difference in nitride island areas between high-G and low-G pixels. Design splits in CMB6 were included to further probe the source of the blue leak. To test the island area hypothesis, one design split of CMB6 has restructured support legs on the high-G devices, which keep the same aspect ratio but significantly reduce the area of the islands. The CMB6 testing apparatus and future experiments intending to use these devices will include versions of eccosorb moats above and below the array pixels to attenuate any remaining out-of-band leak, but low-pass filters used by every planned experiment will render the leak a non-issue.

6. CONCLUSIONS

The TRUCE Collaboration continues to develop feedhorn-coupled dual-polarization sensitive TES bolometer arrays for measurements of CMB polarization anisotropies by several upcoming experiments. The pixels are currently designed for observations centered at 145 GHz, but modifying the on-chip band-defining filters allows for changing the observed bandpass without a complete overhaul of optics and filters upstream from the pixels.

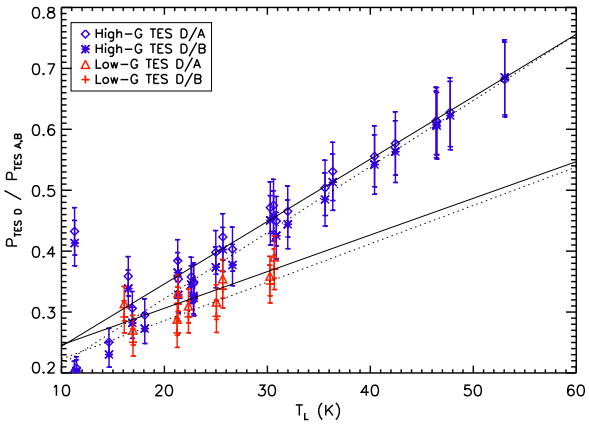

Figure 5. Ratio of out-of-band (TES D) responses to total (TES A or B) responses for both low-G and high-G pixels. Solid (dashed) lines are linear fits to D/A (D/B) responses to load temperature, yielding an estimate of the ratio of nitride island areas between high-G and low-G pixels, which is in agreement with the known value. Fits were performed for $T_{\rm L} > 15$ K to avoid large $\Delta P_{\rm L}$ fluctuations from small thermal variations in the load. Error bars are systematics based on readout calibration uncertainties.

Additionally, the band-defining filters introduce the promising possibility of multichroic monolithic arrays in future designs. We measure devices in the current pixel design to have optical efficiencies of $57 \pm 4\,\mathrm{stat} \pm 9\,\mathrm{sys}$ %. We also observe the devices to have a blue leak in the passband, but the use of eccosorb moats can reduce the absorbed out-of-band power by a factor of roughly two, and all experiments slated to use these devices have plans for in-line optical low-pass filters making any remaining blue passband leak inconsequential. Several modifications included in the next generation of pixels, currently being fabricated, should increase optical efficiencies and decrease absorbed blue leak power.

ACKNOWLEDGMENTS

Work at the University of Colorado is supported by the NSF through grant AST-0705302. Work at Princeton University is supported by Princeton University and the NSF through grants PHY-0355328 and PHY-085587. Work at NIST is supported by the NIST Innovations in Measurement Science program. Work at the University of Chicago is supported by the NSF through grant ANT- 0638937 and the NSF Physics Frontier Center grant PHY-0114422 to the Kavli Institute of Cosmological Physics at the University of Chicago. It also receives generous support from the Kavli Foundation and the Gordon and Betty Moore Foundation.

REFERENCES

1. Kovac, J. M., Leitch, E. M., Pryke, C., Carlstrom, J. E., Halverson, N. W., and Holzapfel, W. L., "Detection of polarization in the cosmic microwave background using DASI," *Nature* **420**, 772–787 (Dec. 2002).
2. Barkats, D., Bischoff, C., Farese, P., Fitzpatrick, L., Gaier, T., Gundersen, J. O., Hedman, M. M., Hyatt, L., McMahon, J. J., Samtleben, D., Staggs, S. T., Vanderlinde, K., and Winstein, B., "First Measurements of the Polarization of the Cosmic Microwave Background Radiation at Small Angular Scales from CAPMAP," *Astrophysical Journal Letters* **619**, L127–L130 (Feb. 2005).
3. Montroy, T. E., Ade, P. A. R., Bock, J. J., Bond, J. R., Borrill, J., Boscaleri, A., Cabella, P., Contaldi, C. R., Crill, B. P., de Bernardis, P., De Gasperis, G., de Oliveira-Costa, A., De Troia, G., di Stefano, G., Hivon, E., Jaffe, A. H., Kisner, T. S., Jones, W. C., Lange, A. E., Masi, S., Mauskopf, P. D., MacTavish, C. J., Melchiorri, A., Natoli, P., Netterfield, C. B., Pascale, E., Piacentini, F., Pogosyan, D., Polenta, G., Prunet, S., Ricciardi, S., Romeo, G., Ruhl, J. E., Santini, P., Tegmark, M., Veneziani, M., and Vittorio, N., "A Measurement of the CMB EE Spectrum from the 2003 Flight of BOOMERANG," *Astrophysical Journal* **647**, 813–822 (2006).

4. Bischoff, C., Hyatt, L., McMahon, J. J., Nixon, G. W., Samtleben, D., Smith, K. M., Vanderlinde, K., Barkats, D., Farese, P., Gaier, T., Gundersen, J. O., Hedman, M. M., Staggs, S. T., and Winstein, B., "New Measurements of Fine-Scale CMB Polarization Power Spectra from CAPMAP at Both 40 and 90 GHz," *Astrophysical Journal* **684**, 771–789 (Sept. 2008).
5. Nolta, M. R., Dunkley, J., Hill, R. S., Hinshaw, G., Komatsu, E., Larson, D., Page, L., Spergel, D. N., Bennett, C. L., Gold, B., Jarosik, N., Odegard, N., Weiland, J. L., Wollack, E., Halpern, M., Kogut, A., Limon, M., Meyer, S. S., Tucker, G. S., and Wright, E. L., "Five-Year Wilkinson Microwave Anisotropy Probe Observations: Angular Power Spectra," *Astrophysical Journal Supplement* **180**, 296–305 (Feb. 2009).
6. Chiang, H. C., Ade, P. A. R., Barkats, D., Battle, J. O., Bierman, E. M., Bock, J. J., Dowell, C. D., Duband, L., Hivon, E. F., Holzapfel, W. L., Hristov, V. V., Jones, W. C., Keating, B. G., Kovac, J. M., Kuo, C. L., Lange, A. E., Leitch, E. M., Mason, P. V., Matsumura, T., Nguyen, H. T., Ponthieu, N., Pryke, C., Richter, S., Rocha, G., Sheehy, C., Takahashi, Y. D., Tolan, J. E., and Yoon, K. W., "Measurement of Cosmic Microwave Background Polarization Power Spectra from Two Years of BICEP Data," *Astrophysical Journal* **711**, 1123–1140 (Mar. 2010).
7. Hu, W. and White, M., "A CMB polarization primer," *New Astronomy* **2**, 323–344 (Oct. 1997).
8. Pryke, C., Ade, P., Bock, J., Bowden, M., Brown, M. L., Cahill, G., Castro, P. G., Church, S., Culverhouse, T., Friedman, R., Ganga, K., Gear, W. K., Gupta, S., Hinderks, J., Kovac, J., Lange, A. E., Leitch, E., Melhuish, S. J., Memari, Y., Murphy, J. A., Orlando, A., Schwarz, R., Sullivan, C. O., Piccirillo, L., Rajguru, N., Rusholme, B., Taylor, A. N., Thompson, K. L., Turner, A. H., Wu, E. Y. S., and Zemcov, M., "Second and Third Season QUaD Cosmic Microwave Background Temperature and Polarization Power Spectra," *Astrophysical Journal* **692**, 1247–1270 (Feb. 2009).
9. Essinger-Hileman, T., Appel, J. W., Beal, J. A., Cho, H. M., Fowler, J., Halpern, M., Hasselfield, M., Irwin, K. D., Marriage, T. A., Niemack, M. D., Page, L., Parker, L. P., Pufu, S., Staggs, S. T., Stryzak, O., Visnjic, C., Yoon, K. W., and Zhao, Y., "The Atacama B-Mode Search: CMB Polarimetry with Transition-Edge-Sensor Bolometers," in [*American Institute of Physics Conference Series*], B. Young, B. Cabrera, & A. Miller, ed., *American Institute of Physics Conference Series* **1185**, 494–497 (Dec. 2009).
10. McMahon, J. J., Aird, K. A., Benson, B. A., Bleem, L. E., Britton, J., Carlstrom, J. E., Chang, C. L., Cho, H. S., de Haan, T., Crawford, T. M., Crites, A. T., Datesman, A., Dobbs, M. A., Everett, W., Halverson, N. W., Holder, G. P., Holzapfel, W. L., Hrubes, D., Irwin, K. D., Joy, M., Keisler, R., Lanting, T. M., Lee, A. T., Leitch, E. M., Loehr, A., Lueker, M., Mehl, J., Meyer, S. S., Mohr, J. J., Montroy, T. E., Niemack, M. D., Ngeow, C. C., Novosad, V., Padin, S., Plagge, T., Pryke, C., Reichardt, C., Ruhl, J. E., Schaffer, K. K., Shaw, L., Shirokoff, E., Spieler, H. G., Stadler, B., Stark, A. A., Staniszewski, Z., Vanderlinde, K., Vieira, J. D., Wang, G., Williamson, R., Yefremenko, V., Yoon, K. W., Zhan, O., and Zenteno, A., "SPTpol: an instrument for CMB polarization," in [*American Institute of Physics Conference Series*], B. Young, B. Cabrera, & A. Miller, ed., *American Institute of Physics Conference Series* **1185**, 511–514 (Dec. 2009).
11. Niemack, M. D., Ade, P. A. R., Aguirre, J., Barrientos, F., Beall, J. A., Bond, J. R., Britton, J., Cho, H. M., Das, S., Devlin, M. J., Dicker, S., Dunkley, J., Dunner, R., Fowler, J. W., Hajian, A., Halpern, M., Hasselfield, M., Hilton, G. C., Hilton, M., Hubmayr, J., Hughes, J. P., Infante, L., Irwin, K. D., Jarosik, N., Klein, J., Kosowsky, A., Marriage, T. A., McMahon, J., Menanteau, F., Moodley, K., Nibarger, J. P., Nolta, M. R., Page, L. A., Partridge, B., Reese, E. D., Sievers, J., Spergel, D. N., Staggs, S. T., Thornton, R., Tucker, C., Wollack, E., and Yoon, K. W., "ACTPol: A polarization-sensitive receiver for the Atacama Cosmology Telescope," *ArXiv e-prints* (June 2010).
12. Austermann, J. E., Niemack, M. D., Appel, J. W., Beall, J. A., Becker, D., Bennett, D. A., Benson, B. A., Bleem, L. E., Britton, J., Carlstrom, J. E., Chang, C. L., Cho, H. M., Crites, A. T., Essinger-Hileman, T., Everett, W., Halverson, N. W., Henning, J. W., Hilton, G. C., Irwin, K. D., McMahon, J., Mehl, J., Meyer, S. S., Parker, L. P., Simon, S. M., Staggs, S. T., Ullom, J. N., Visnjic, C., Yoon, K. W., and Zhao, Y., "Measurements of Bolometer Uniformity for Feedhorn Coupled TES Polarimeters," in [*American Institute of Physics Conference Series*], B. Young, B. Cabrera, & A. Miller, ed., *American Institute of Physics Conference Series* **1185**, 498–501 (Dec. 2009).

13. Yoon, K. W., Appel, J. W., Austermann, J. E., Beall, J. A., Becker, D., Benson, B. A., Bleem, L. E., Britton, J., Chang, C. L., Carlstrom, J. E., Cho, H., Crites, A. T., Essinger-Hileman, T., Everett, W., Halverson, N. W., Henning, J. W., Hilton, G. C., Irwin, K. D., McMahon, J., Mehl, J., Meyer, S. S., Moseley, S., Niemack, M. D., Parker, L. P., Simon, S. M., Staggs, S. T., U-Yen, K., Visnjic, C., Wollack, E., and Zhao, Y., "Feedhorn-Coupled TES Polarimeters for Next-Generation CMB Instruments," in [*American Institute of Physics Conference Series*], B. Young, B. Cabrera, & A. Miller, ed., *American Institute of Physics Conference Series* **1185**, 515–518 (Dec. 2009).
14. Bock, J. J., *Rocket-borne observation of singly ionized carbon 158 micron emission from the diffuse interstellar medium*, PhD thesis, California Univ. (1994).
15. Emerson and Cuming Microwave Products, http://www.eccosorb.com
16. Hemmati, H., Mather, J. C., and Eichhorn, W. L., "Submillimeter and millimeter wave characterization of absorbing materials," *Applied Optics* **24**, 4489–4492 (Dec. 1985).
17. Mather, J. C., Fixsen, D. J., Shafer, R. A., Mosier, C., and Wilkinson, D. T., "Calibrator Design for the COBE Far-Infrared Absolute Spectrophotometer (FIRAS)," *Astrophysical Journal* **512**, 511–520 (Feb. 1999).
18. Bleem, L. E., Appel, J. W., Austermann, J. E., Beall, J. A., Becker, D. T., Benson, B. A., Britton, J., Carlstrom, J. E., Chang, C. L., Cho, H. M., Crites, A. T., Essinger-Hileman, T., Everett, W., Halverson, N. W., Henning, J. W., Hilton, G. C., Irwin, K. D., McMahon, J., Mehl, J., Meyer, S. S., Niemack, M. D., Parker, L. P., Simon, S. M., Staggs, S. T., Visnjic, C., Yoon, K. W., and Zhao, Y., "Optical properties of Feedhorn-coupled TES polarimeters for CMB polarimetry," in [*American Institute of Physics Conference Series*], B. Young, B. Cabrera, & A. Miller, ed., *American Institute of Physics Conference Series* **1185**, 479–482 (Dec. 2009).
19. Thomas Keating Instruments, http://www.terahertz.co.uk.